

# Soft Matter

Accepted Manuscript



This is an *Accepted Manuscript*, which has been through the Royal Society of Chemistry peer review process and has been accepted for publication.

*Accepted Manuscripts* are published online shortly after acceptance, before technical editing, formatting and proof reading. Using this free service, authors can make their results available to the community, in citable form, before we publish the edited article. We will replace this *Accepted Manuscript* with the edited and formatted *Advance Article* as soon as it is available.

You can find more information about *Accepted Manuscripts* in the [Information for Authors](#).

Please note that technical editing may introduce minor changes to the text and/or graphics, which may alter content. The journal's standard [Terms & Conditions](#) and the [Ethical guidelines](#) still apply. In no event shall the Royal Society of Chemistry be held responsible for any errors or omissions in this *Accepted Manuscript* or any consequences arising from the use of any information it contains.



## Magnetophoresis of superparamagnetic nanoparticle at low field gradient: Hydrodynamic effect

Sim Siong Leong<sup>a</sup>, Zainal Ahmad<sup>a</sup>, JitKang Lim<sup>\*a,b</sup>

Received 00th January 20xx,  
Accepted 00th January 20xx

DOI: 10.1039/x0xx00000x

www.rsc.org/

Convective current driven by momentum transfer between the magnetic nanoparticles (MNPs) and its surrounding fluid during the magnetophoresis process under low gradient magnetic field (<100 T/m) was presented. This magnetophoresis induced convective flow, which imposed direct hydrodynamic effects onto the separation kinetic of MNPs under low gradient magnetic separation (LGMS), is analogous to the natural convection found in heat transportation. Here, we show the significance of the induced convection in dictating the transport behavior of MNPs even at very low particle concentration of 5 mg/L and this feature can be characterized by newly defined magnetic Grashof number. By incorporating the fluid flow equations into the existing magnetophoresis model, we revealed two unique features of the convective flow which associated to the low gradient magnetophoresis, namely (1) the continuous homogenization of MNPs solution and (2) accompanying sweeping flow that speed-up the MNPs collection. According to both simulation and experimental data, the induced convection boost the magnetophoretic capture of MNPs by approximately 30 times compared to the situation with no occurrence of convection.

### 1 Introduction

In recent years, magnetic nanoparticles (MNPs) have been emerged as one of the most versatile nanomaterial with huge potential for various biomedical<sup>1-6</sup> and environmental applications.<sup>7-11</sup> For separation processes are concerned, the usages of MNP is basically operated at such a way: MNPs, which have been surface functionalized, are initially dispersed into the solution which contains targeting compounds such that MNPs can be tagged onto the aforementioned compounds either through specific or non-specific binding. Next, the MNPs tagged compound are withdrawn from the solution or directed to a specific region in a controlled manner by an externally applied magnetic field.<sup>12</sup> This scheme allows the separation of non-magnetic compound by a process known as magnetophoresis which involves the controlled motion of

MNPs under externally applied magnetic field in relative to the surrounding fluid.<sup>13</sup>

There are numerous benefits associated to the use of MNPs in promoting the separation of biological component as compared to conventional separation processes.<sup>14</sup> However, since MNPs are extremely small, collection of them from surrounding media poses great challenges due to significant perturbation of their magnetophoretic pathway by thermal energy and viscous drag.<sup>15</sup> Henceforth, high gradient magnetic field is applied such that MNPs attain large magnetophoretic force to overcome these randomization energy and opposing force(s) in order to achieve separation in a reasonable time scale. This process is known as high gradient magnetic separation (HGMS)<sup>16</sup> which encounters four significant drawbacks as follows: (1) high purchase and installation cost,<sup>17</sup> (2) complexity in developing analytical solutions due to the highly inhomogeneous magnetic field inside the HGMS column,<sup>16</sup> (3) high tendency of MNPs deposition on wires within the HGMS column which causes the reduction of separation efficiency or even brings about permanent retention of MNPs in the column,<sup>14</sup> and (4) energy losses due to Joule effect during magnetization and demagnetization of the magnetizable wires.<sup>18</sup>

Lately, Yavuz and co-workers demonstrated the feasibility of low gradient magnetic field generated by permanent magnet (magnetic flux density gradient  $\nabla B < 100$  T/m) in the collection of 10 nm superparamagnetic magnetite nanocrystals.<sup>19</sup> Successful implementation of this separation method, which is known as low gradient magnetic separation (LGMS), was identified to be contributed by the formation of field-induced aggregates.<sup>12, 19</sup> This reversible aggregation has greatly altered the dynamical behavior of LGMS by accelerating MNPs collection and reducing separation time. Due to its simplicity and cost-effectiveness,<sup>17</sup> many current

<sup>a</sup> School of Chemical Engineering, Universiti Sains Malaysia, Nibong Tebal, Penang 14300, Malaysia.

<sup>b</sup> Department of Physics, Carnegie Mellon University, Pittsburgh, PA 15213, USA.

† Footnotes relating to the title and/or authors should appear here.

Electronic Supplementary Information (ESI) available: S1 provides a justification for the validity of Beer-Lambert law in this study. S2 illustrates the calculation to justify the amount of MB is overwhelming that of MNPs in dye-tracing experiment described in Section 2.3. S3 shows detailed analysis of magnetic Bjerrum length and aggregation parameter for MNPs system employed in current work. S4 demonstrates the magnetic flux density of the cylindrical magnet in three dimensional space and justify the suitability of one dimensional magnetic flux density approximation in current work. S5 and S6 gives more detailed description on the simulation of non MNPs/Fluid interacting magnetophoresis model and hydrodynamically interacting magnetophoresis model respectively by providing the discussion on initial and boundary conditions involved in the simulation. S7 provides the list of symbols used in current work along with their units. Supplementary video serves to make a clearer illustration on the difference between the simulation results from the both models developed in this work. See DOI: 10.1039/x0xx00000x

research efforts are dedicated to study the underlying principles that define the transport behavior of MNPs under LGMS.<sup>20-26</sup> By taking interparticle interaction between MNPs (which is known as MNPs/MNPs interaction in this article) into consideration, MNPs' motion under LGMS has been described quantitatively to predict the separation kinetic profile.<sup>12, 20, 21, 25</sup> Furthermore, the morphology of MNPs aggregation under LGMS has been investigated and explained by including magnetic interaction into the classical Derjaguin-Landau-Verwey-Overbeek (DLVO) theory.<sup>22</sup> Also, the transient behavior of MNPs aggregation upon the application of external magnetic field has been studied and simulated.<sup>24</sup>

While MNPs/MNPs interaction is studied comprehensively, the interaction between MNPs and surrounding fluid, which is contributed by the momentum transfer through the collision between both species, has been neglected by most researchers who are working on LGMS system.<sup>20, 21, 25, 26</sup> There are very few existing literature reported this type of interaction, which is termed as MNPs/Fluid interaction in this article. Since most of the engineering applications of MNPs involve the controlled magnetophoretic movement of MNPs suspended in fluid,<sup>5, 6, 8, 9, 27-29</sup> it is reasonable to hypothesize that MNPs/Fluid interaction is inevitable and playing an essential role in dictating the LGMS kinetics. Microscopically, the magnetophoretic separation of MNPs in microfluidic systems, where MNPs experience highly localized magnetic field gradient, has been studied and simulated theoretically by taking MNPs/Fluid interaction into consideration.<sup>30-34</sup> From the works of Furlani and coworkers on microfluidic system, it was observed that the local fluid flow is heavily influenced by magnetophoretic motion of MNPs,<sup>32</sup> which leads us to believe that MNPs/Fluid interaction also has the pronounced effect on the LGMS process. Yet, there is almost no discussion on the macroscopic effect of MNPs/Fluid interaction on LGMS that is widely utilized in various engineering applications. In conjunction with this situation, we intended to complete the physical understanding on the magnetophoretic behavior of MNPs under LGMS by investigating how MNPs/Fluid interaction influences LGMS performance.

In this work, dilute MNPs solution was utilized such that MNPs/MNPs interaction is negligible and can be safely ignored in the result analysis. Initially, magnetophoresis experiment was carried out to study the kinetic behavior of MNPs solution which is subjected to low gradient magnetic field. Next, two different models were developed to describe low gradient magnetophoresis of MNPs. In the first model, classical assumption was made by taking motion of MNPs is solely governed by magnetic, viscous, gravitational and Brownian forces while the fluid remains stagnant and unaltered by the MNPs motion at all time. Later in the second model, the drift-diffusion equation was coupled and solved together with fluid flow equations with the assumption that the surrounding fluid of MNPs is no longer stagnant but can be perturbed by MNPs' motion. The simulation results from both models were compared with the experimental result in order to justify the importance of hydrodynamic effect originated from MNPs/Fluid interaction in dictating the LGMS process. Furthermore, magnetic Grashof number was developed to characterize the significance of magnetophoresis induced convection under LGMS in dimensionless form.

## 2 Experimental section

### 2.1 Characterization of magnetic nanoparticles (MNPs)

**Transmission electron microscopy (TEM).** MNPs solution used in this experiment was purchased from Ocean NanoTech, consisting of aqueous suspension of iron oxide nanoparticle coated with polyethylene glycol (PEG). TEM was used to capture the images of the MNPs. The images captured enable us to determine the geometrical shape and magnetic core size of MNPs. A droplet of dilute MNPs solution (~ 20 mg/L) was deposited and dried on a carbon grid for 30 minutes. The dried MNPs, which were immobilized on the carbon grid, were observed by using TEM (JEOL, JEM-20CX).

**Dynamics light scattering (DLS).** DLS technique was employed to determine the hydrodynamic size of MNPs.<sup>35</sup> Before performing DLS analysis, the received MNPs solution was diluted to 10 mg/L such that the effects of multiple scattering and particles interaction can be minimized during the measurement. The fluctuation of the scattered light intensity was detected and measured at an angle of 173° to the incident light (Malvern Instruments Zetasizer ZS). The transient light intensity fluctuation was fitted into a correlation function which decays exponentially with time. The correlation function decays more rapidly for the smaller MNPs as light intensity fluctuation is greater due to the faster diffusion of small MNPs. Cumulants method was employed to analyze the correlation function so that the translational diffusivity of MNPs suspended in the solution is obtained. Next, according to MNPs' translational-diffusivity, hydrodynamic size of MNPs was inferred by using Einstein-Stokes equation. Hence, in this analysis, all MNPs were assumed to be spherical in shape.

**Vibrating sample magnetometer (VSM).** VSM was used to characterize magnetic response of MNPs. In order to perform VSM measurement, 0.0006 g of MNPs was dispersed in an epoxy forming a cast epoxy sample. The cast epoxy sample was attached to a vibrating glass rod that was in the center of an electromagnetic direct current (DC) field. The magnetic response of the sample was measured with the full sweep for both the positive and negative field components with digitally controlled field stepping and data averaging.

### 2.2 Magnetophoresis kinetics measurement

The experimental setup is illustrated in Fig. 1. A standard 1 × 1 × 1 cm disposable cuvette was filled with 3 mL of homogeneous MNPs solution such that the solution surface is measured 3 cm vertically from the cuvette's base. Next, the cuvette is located on top of a cylindrical neodymium boron ferrite (NdFeB) magnet. The NdFeB magnet is N50-graded with remanence magnetization of 1.45 T and was obtained from Ningbo YuXiang E&M Int'l Co, Ltd. UV-vis spectrophotometer (Agilent Cary-60) was employed to measure concentration of MNPs in solution where monochromatic light with wavelength of 530 nm was passed through MNPs solution and light absorbance was recorded. The initial MNPs concentration was varied, within the range from 10 to 100 mg/L, to probe the particle concentration effect on the magnetophoresis kinetics. Next, the light absorbance was recorded in different locations along the cuvette

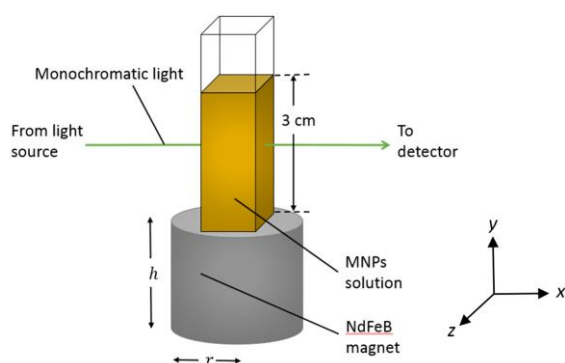


**Fig. 1** Setup of magnetophoresis experiment. Initially, a cuvette was filled with homogeneously dispersed MNPs solution and was placed on a grade N50 NdFeB cylindrical permanent magnet with remanent magnetization of 1.45 T, which radius and height of the magnet are given by 0.7 cm and 1.5 cm respectively. The light absorbance of the MNPs solution was measured, every 5 minutes after the magnetophoresis started, by using UV-vis spectrophotometer and the result was used to infer MNPs concentration.

such that the whole picture of the magnetophoresis kinetics can be captured. As Beer-Lambert Law was proven to be valid for MNPs concentration range employed in this study (see Supplementary Information S1 for justification), normalized MNPs concentration (with respect to initial concentration of MNPs solution before the magnetophoresis experiment begins) was calculated as follows:

$$c_{N,MNPs} = \frac{A - A_o}{A_i - A_o} \quad (1)$$

where  $A$  is light absorbance of MNPs solution,  $A_o$  is the light absorbance of the blank solution and  $A_i$  is the initial light absorbance of MNPs solution.

### 2.3 Dye-tracing experiment

This experiment was performed to trace fluid motion visually during magnetophoresis. Initially, approximately 3000 mg/L of concentrated Methylene Blue (MB) was introduced carefully to the bottom of a cuvette containing 3 mL of MNPs solution by using a syringe. The MNPs solution was then subjected to magnetophoresis and the motion of the dye in the solution was captured. As dye molecules are highly positively charged and MNPs have average zeta potential of  $-10$  mV, it is believed that some of the dye molecules might adhere to MNPs due to electrostatic interaction.<sup>36</sup> However, since we have over supplied the MB molecules, there should be significant amount of freely suspended dye molecules which can trace the fluid motion within MNPs solution associated to magnetophoresis visually (see Supplementary Information S2 for justification). The procedure above was carried out by using MNPs solution with the following concentrations: 0 (blank solution which was used as the controlled experiment), 5, 10, 20, 50, 100 mg/L. The dye motion in the MNPs solution with different concentration under magnetophoresis was compared.

## 3 Theoretical model

In this study, two models were developed to predict the separation kinetic profile of magnetophoresis in the experiment described above, namely non MNPs/Fluid interacting and hydrodynamically interacting magnetophoresis models. The prediction from both models were then compared with the experimental result to verify the accuracy of the models and hence justify the importance of hydrodynamic interaction in low gradient magnetophoresis of MNPs.

### 3.1 Non MNPs/Fluid interacting magnetophoresis model

Several assumptions were made in the development of this model (1) MNPs are distributed uniformly throughout the solution prior to the application of magnetic field, (2) MNPs/MNPs interaction is negligible due to the non-interactive nature of the particle system (see Supplementary Information S3 for justification), (3) MNPs are spherical in shape which consists of magnetic core surrounded by layer of non-magnetic polyethylene glycol (PEG), (4) magnetophoretic migration of MNPs in the solution is creeping motion which obeys Stokes' law, (5) the motion of MNPs does not create any fluid flow perturbation such that the surrounding fluid remains stagnant throughout the entire course of magnetophoresis and (6) vertical component of magnetic flux density gradient, throughout the MNPs solution subjected to magnetophoresis, is far more dominant compared to its horizontal counterpart (see Supplementary Information S4 for more detailed justification).

Under an external magnetic field, there are four forces acting on MNPs which govern the motion of MNPs in the MNPs solution: (1) magnetic force, due to the response of magnetic dipole moment in MNPs to the externally applied magnetic field, (2) viscous drag force, due to the resistance contributed by the relative motion of MNPs in the solution, (3) gravitational force and (4) Brownian force which induces the diffusion of MNPs along the MNPs concentration gradient and is originated from thermal motion. The transport behaviour of MNPs in the fluid throughout magnetophoresis, due to the combination of diffusion and fluid advection effects, is described by drift-diffusion equation:<sup>37</sup>

$$\frac{\partial c}{\partial t} = D \nabla^2 c - \nabla \cdot (\mathbf{u}c) \quad (2)$$

where  $c$  is concentration of MNPs solution,  $\mathbf{u}$  is magnetophoretic velocity of MNPs and  $D$  is diffusivity of MNPs in the solution which can be calculated by using Einstein-Stokes equation:<sup>15</sup>

$$D = \frac{k_B T}{6\pi\eta R_h} \quad (3)$$

where  $k_B$  is Boltzmann constant,  $T$  is absolute temperature,  $\eta$  is dynamic viscosity of fluid and  $R_h$  is hydrodynamic radius of MNPs ( $= 21.5 \times 10^{-9}$  m). The first term on the right hand side of Equation (2) depicts the transport of MNPs in the solution due to thermal motion of particles. Whereas, the second term represents the divergence of MNPs flux which is induced by magnetic, viscous and gravitational forces acting on each individual MNP during magnetophoresis. According to Newton's second law of motion, the

acceleration of MNPs  $du/dt$  is dependent on the sum of all forces that are acting on it:

$$m_p \frac{du}{dt} = \mathbf{F}_{mag} + \mathbf{F}_d + \mathbf{F}_g \quad (4)$$

where  $m_p$  is mass of a MNP,  $\mathbf{F}_{mag}$  is magnetic force,  $\mathbf{F}_d$  is viscous drag force and  $\mathbf{F}_g$  is gravitational force. The inertial term ( $m_p \frac{du}{dt}$ ) is negligible under low Reynold number flow and hence, for simplicity, it is neglected in the present analysis.<sup>37</sup> Based on this assumption, Equation (4) finally turns out to be

$$0 = \mathbf{F}_{mag} + \mathbf{F}_d + \mathbf{F}_g \quad (5)$$

Magnetic force  $\mathbf{F}_{mag}$  acting on a MNP is formulated by:<sup>12</sup>

$$\mathbf{F}_{mag} = \mu \nabla B \quad (6)$$

where  $\mu$  is magnetic dipole moment and  $B$  is magnetic flux density. For an axially magnetized cylindrical magnet, the magnetic flux density along the axis of the magnet, where vertical distance from magnet pole face is given by  $y$ , can be calculated as follows:<sup>38</sup>

$$B = \frac{B_r}{2} \left[ \frac{y+h}{\sqrt{(y+h)^2 + r^2}} - \frac{y}{\sqrt{y^2 + r^2}} \right] \quad (7)$$

where  $B_r$  is remanent magnetic flux density,  $h$  is height of cylindrical magnet and  $r$  is radius of cylindrical magnet. We consider that the variation of magnetic flux density along the radial direction is insignificant compared to that of the axial direction (Assumption 6),  $x$ - and  $z$ - components of  $\nabla B$  are negligible and  $\nabla B$  is thus can be approximated as:

$$\nabla B \approx \frac{\partial B}{\partial y} \mathbf{e}_y = \frac{B_r r^2}{2} \left[ \frac{1}{[(y+h)^2 + r^2]^{3/2}} - \frac{1}{[y^2 + r^2]^{3/2}} \right] \mathbf{e}_y \quad (8)$$

where  $\mathbf{e}_y$  is the unit vector pointing to the positive  $y$ -direction. On the other hand, magnetic dipole moment is given by:

$$\mu = m_p M_{p,m} \quad (9)$$

where  $M_{p,m}$  is the mass magnetization of MNPs which is the function of magnetic field strength  $H$  that applied on it. The relationship between the mass magnetization of MNPs and the applied magnetic field strength can be obtained by fitting the magnetization curve, obtained from VSM, to the following equation:<sup>39</sup>

$$M_{p,m} = M_s L \left( \frac{mH}{k_B T} \right) = M_s \left[ \coth \left( \frac{mH}{k_B T} \right) - \frac{k_B T}{mH} \right] \quad (10)$$

where  $M_s$  is the saturation magnetization per unit mass of MNPs,  $m$

is the strength of magnetic moment for one magnetic dipole and  $L$  is the Langevin function  $[L(x) = \coth(x) - 1/x]$ . Since relative permeability of water is approaching to unity, the relationship between magnetic flux density and magnetic field strength in the aqueous MNPs solution is given by:

$$B = \mu_0 H \quad (11)$$

By inserting Equation (7) to (11) into Equation (6), the magnetic force acting on a MNP can be expressed as a function of distance (along the axial or vertical direction  $y$ ) from the magnet pole as below:

$$\mathbf{F}_{mag} = \left( m_p M_s L \left\{ \frac{m B_r}{2 \mu_0 k_B T} \left[ \frac{y+h}{\sqrt{(y+h)^2 + r^2}} - \frac{y}{\sqrt{y^2 + r^2}} \right] \right\} \times \frac{B_r r^2}{2} \left[ \frac{1}{[(y+h)^2 + r^2]^{3/2}} - \frac{1}{[y^2 + r^2]^{3/2}} \right] \right) \mathbf{e}_y \quad (12)$$

The viscous drag force experienced by a MNP which is moving in a viscous fluid (or under low Reynold number environment) is formulated by Stokes' law, which is given by:<sup>25</sup>

$$\mathbf{F}_d = -6\pi\eta r_h \mathbf{u} = -6\pi\eta R_h (u_x \mathbf{e}_x + u_y \mathbf{e}_y + u_z \mathbf{e}_z) \quad (13)$$

where  $u_x$ ,  $u_y$  and  $u_z$  are  $x$ -,  $y$ - and  $z$ -components of MNP's magnetophoretic velocity respectively. Also,  $\mathbf{e}_x$  and  $\mathbf{e}_z$  are the unit vectors pointing to positive  $x$ - and  $z$ -directions.

The gravitational force acting on a MNP is given by Newton's Law of gravitation:

$$\mathbf{F}_g = -m_p \mathbf{g} = -m |\mathbf{g}| \mathbf{e}_y \quad (14)$$

where  $\mathbf{g}$  is gravitational acceleration vector and  $|\mathbf{g}|$  is magnitude of gravitational acceleration ( $\approx 9.81$  m/s<sup>2</sup> on Earth surface).

By incorporating Equations (12) to (14) into Equation (5) Equations (15) are obtained, as shown below. Upon rearrangement,  $x$ -,  $y$ - and  $z$ - components of magnetophoretic velocity of MNP subjected to magnetophoresis in the model system are given by Equations (16).

Equations (16) are required to solve Equation (2) in order to predict the transient behavior and generate separation kinetic profile of magnetophoresis process. (Please refer to Supplemental Information S5 for the details of computer simulation, including initial and boundary conditions employed in this model)

$$-6\pi\eta r_h u_x = 0 \quad (15a)$$

$$\left( m_p M_s L \left\{ \frac{m B_r}{2 \mu_0 k_B T} \left[ \frac{y+h}{\sqrt{(y+h)^2 + r^2}} - \frac{y}{\sqrt{y^2 + r^2}} \right] \right\} \times \frac{B_r r^2}{2} \left[ \frac{1}{[(y+h)^2 + r^2]^{3/2}} - \frac{1}{[y^2 + r^2]^{3/2}} \right] \right) - m_p |\mathbf{g}| - 6\pi\eta R_h u_y = 0 \quad (15b)$$

$$-6\pi\eta r_h u_z = 0 \quad (15c)$$

$$u_x = 0 \quad (16a)$$

$$u_y = \frac{\left( m_p M_s L \left\{ \frac{m B_r}{2 \mu_0 k_B T} \left[ \frac{y+h}{\sqrt{(y+h)^2 + r^2}} - \frac{y}{\sqrt{y^2 + r^2}} \right] \right\} \times \frac{B_r r^2}{2} \left[ \frac{1}{[(y+h)^2 + r^2]^{3/2}} - \frac{1}{[y^2 + r^2]^{3/2}} \right] \right) - m_p |g|}{6 \pi \eta R_h} \quad (16b)$$

$$u_z = 0 \quad (16c)$$

### 3.2 Hydrodynamically interacting magnetophoresis model

In the previous model, the fluid is assumed to be stagnant and remains unaltered by the motion of MNPs throughout the magnetophoresis process. In the second model, this assumption has been relaxed such that fluid flow could be generated within MNPs solution due to MNPs/Fluid interaction. Similar to the non MNPs/Fluid interacting magnetophoresis model, the magnetophoresis of MNPs is also governed by drift-diffusion equation stated in Equation (2). However in hydrodynamically interacting magnetophoresis model, the momentum obtained by MNPs due to the response of magnetic dipoles to the external magnetic field, is allowed to be transferred to the surrounding fluid as a consequence of the viscous property possessed by the fluid. Hence, Equations (16) are no longer valid in predicting magnetophoretic velocity of MNPs. On the contrary, the convective motion of the MNPs solution is calculated by the well-known Continuity and Navier-Stokes equations:<sup>40</sup>

$$\nabla \cdot \mathbf{u} = 0 \quad (17)$$

$$\rho \left( \frac{\partial \mathbf{u}}{\partial t} + \mathbf{u} \cdot \nabla \mathbf{u} \right) = -\nabla p + \eta \nabla^2 \mathbf{u} + \rho \mathbf{g} + \mathbf{f}_m \quad (18)$$

By including Navier-Stokes equation into this model, momentum transfer due to MNPs/Fluid interaction has been incorporated accordingly. Equations (17) and (18) govern the momentum transfer within the MNPs solution by connecting its spatial fluid flow profile to viscosity and external forces imposed onto it, namely magnetic and gravitational forces. Besides, the MNPs solution is assumed to be an incompressible fluid which is valid under atmospheric pressure. Here,  $\mathbf{u}$  is the velocity vector of the MNPs solution,  $\rho$  is density of MNPs solution,  $p$  is absolute pressure and  $\mathbf{f}_m$  is

volumetric magnetic force acting on MNPs solution. The last term in Equation (18) represents the magnetic force acting on unit volume of MNPs solution due to the application of the external magnetic field. In other words, it is equivalent to the rate of momentum transfer into a unit volume of MNPs solution due to the collective response of this portion of solution to the external magnetic field. Hence,  $\mathbf{f}_m$  is a function of volumetric magnetization of MNPs solution  $M$  and magnetic flux density gradient  $\nabla B$  and can be defined as such:

$$\mathbf{f}_m = M \nabla B \quad (19)$$

Here, volumetric magnetization of MNPs solution  $M$  is dependent on the concentration of MNPs  $c$  in the solution:

$$M = c M_{p,m} \quad (20)$$

where  $M_{p,m}$  is mass magnetization of MNPs as given in Equation (10). (Please refer to Supplementary Information S6 for the details of computer simulation, including initial and boundary conditions employed in this model)

## 4 Results and discussion

### 4.1 Characterization of magnetic nanoparticles (MNPs)

Based on image analysis performed on 136 MNPs captured by transmission electron microscopy, the average core size was determined as  $30.94 \pm 2.18$  nm. In addition, it can be observed that the MNPs were almost spherical in shape (Fig. 2a). Nevertheless, the average MNPs hydrodynamic diameter was being measured by dynamic light scattering (DLS) (Malvern Instruments Nanosizer ZS) and it was determined as 43 nm, which is roughly 12 nm larger than

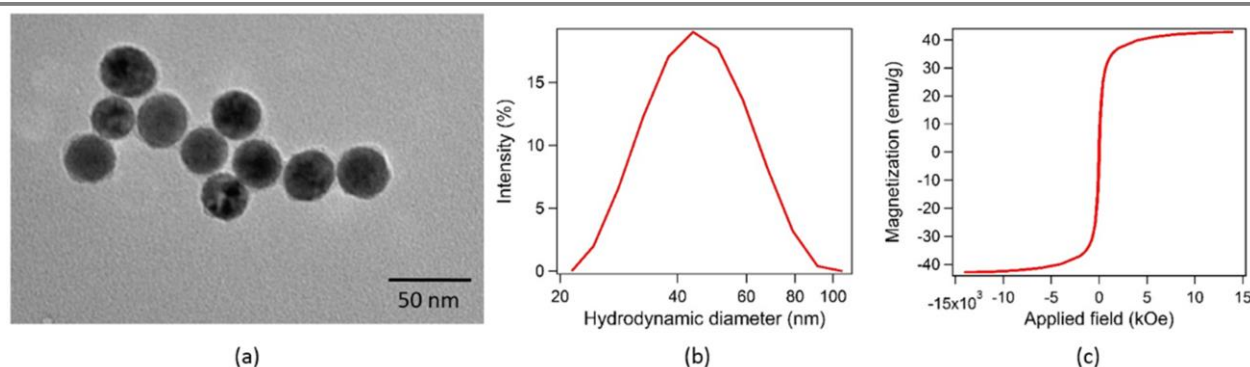


**Fig. 2** (a) Transmission electron micrograph (TEM) of MNPs. It can be observed that MNPs are nearly spherical and the magnetic core size is approximately 30 nm. This result has justified information provided by the supplier. A layer of PEG coating that surrounds MNPs is also noticeable. The aggregation of MNPs shown in this figure is due to the drying of the MNPs solution on the carbon grid prior to the TEM analysis. (b) Hydrodynamic size distribution of MNPs in the solution provided by DLS measurement. (c) Magnetization curve of MNPs used in this study.

their particle core size due to the PEG coating (Fig. 2b).<sup>35</sup> The non-hysteretic behavior of the magnetization curve, which is recorded by vibrating sample magnetometer (VSM) (ARKival ADE/DMS Model 880) measurement, clearly indicates the superparamagnetic nature of this MNPs with its saturation magnetization at 42.7 emu/g (Fig. 2c).<sup>38</sup>

#### 4.2 Magnetophoresis kinetics profile

Under the influence of external magnetic field generated by a grade N50 NdFeB cylindrical permanent magnet (1.4 cm in diameter and 1.5 cm in length) with remanence magnetization of 1.45 T, suspended MNPs were attracted towards the bottom of the solution by magnetic force rendering MNPs concentration in the solution decreases in tandem with time advancement (Fig. 1). Fig. 3a illustrates that the normalized separation kinetic profiles of the MNPs solution almost collapse into a single curve regardless of the initial particle concentration used. This observation revealed the concentration effects, namely MNPs/MNPs interaction, is insignificant in dictating the kinetic of magnetophoresis under LGMS. Rationally, the MNPs/MNPs interaction is more intense in higher concentrated MNPs solution due to higher collision frequency which subsequently leads to the formation of larger aggregate within a shorter period. The larger aggregate should be more magnetically responsive, and hence achieves higher magnetophoretic velocity and speed-up the collection of MNPs under magnetophoresis.<sup>19, 20, 26</sup> Such concentration dependency of separation kinetic profile has been observed in our previous work which intensively interacting MNPs system were used.<sup>41, 42</sup> However, the independence of separation kinetic profile on MNPs concentration (Fig. 3a) leads us to deduce that the MNPs concentration range employed in this work (10 to 100 mg/L) is still far below the critical MNPs concentration in which interparticle interaction starts to become significant. In addition, according to the theory developed by Andreu and coworkers,<sup>24</sup> magnetic interaction between MNPs is relevant only when the aggregation parameter  $N^*$  is larger than unity. For instance, the largest value of  $N^*$  considered in this work is given by 0.158 when MNPs solution with concentration of 100 mg/L was used (see supplementary information S3 for full details of calculation). Aggregation parameter  $N^*$  should be much lower than this value in other cases in which particle concentration is below 100 mg/L. As  $N^*$  values are well below unity within the concentration range (10 – 100 mg/L) considered in the current work, it can be concluded that magnetic interaction between MNPs and reversible aggregation is negligible. Since the ultimate goal of this work is to study the nature of MNPs/Fluid interaction under LGMS, this MNPs system is ideal and well-suited for the current investigation with MNPs/MNPs interaction is negligible and can be excluded.

Coincidentally, separation kinetic profiles measured at different locations throughout the MNPs solution have also collapsed onto a single curve (Fig. 3b). This observation indicates that MNPs were uniformly distributed throughout the MNPs solution during the real time magnetophoresis process as MNPs concentrations at different locations in the solution are similar within the entire time scale of the experiment. Under this circumstance, the MNPs solution in the cuvette remains homogeneous while undergoing magnetophoresis.

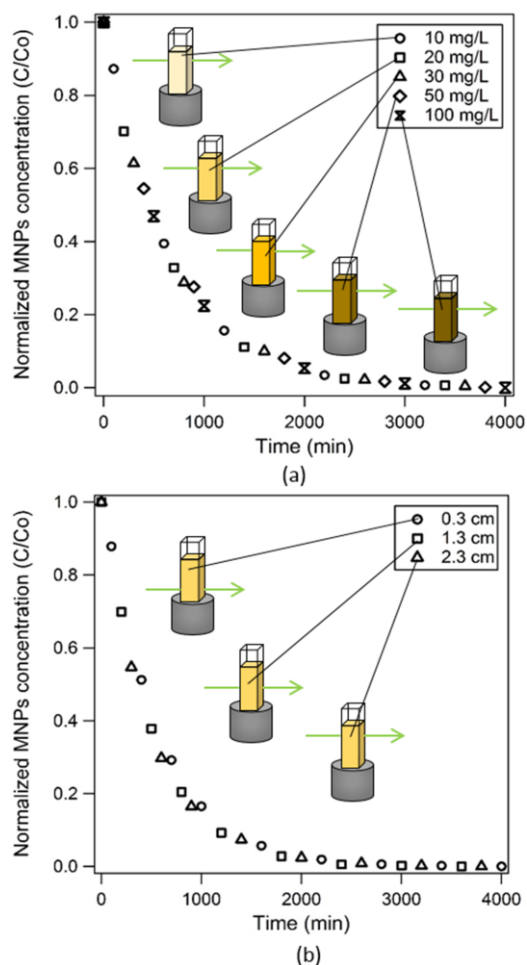


**Fig. 3** (a) Separation kinetic profiles for experiments which employ MNPs solution with different initial concentration (ranging from 10 to 100 mg/L). The measurement was taken at position where vertically 2.3 cm away from the bottom of the MNPs solution. (b) Separation kinetic profiles at different vertical positions (0.3, 1.3 and 2.3 cm from the bottom of the MNPs solution respectively). 20 mg/L of MNPs solution was used in this experiment.

The time-lapse photos captured while MNPs solution was undergoing magnetophoresis (Fig. 4) further verify this argument. This experimental observation provided the first evidence which suggests the importance of hydrodynamic effect associated to magnetophoresis, which is the subject of discussion in the following sections.

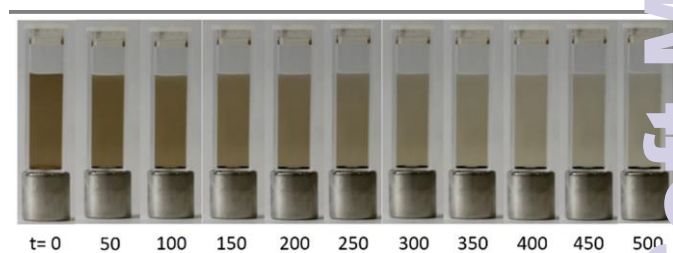


**Fig. 4** Time lapse images of MNPs solution captured in real time during magnetophoresis experiment. The unit of time  $t$  is minutes

### 4.3 Non MNPs/Fluid interacting magnetophoresis

As shown in the time lapse images of the simulation results in Fig. 5a, non MNPs/Fluid interacting model predicted progressive clearing of MNPs at the bottom of the cuvette where the magnetic flux density gradient is the highest. Rationally, simulation result displays such behavior because of the spatial resolution of magnetic flux density gradient from the magnet pole,<sup>43</sup> which causes MNPs located closer to the magnet experience much greater magnetophoretic force and hence migrates at a faster speed to the magnetic source compared to those located further away from the magnet.<sup>15</sup> For instance, a MNP with diameter of 30 nm located 1 mm away from the magnet pole face experiences magnetic flux density gradient  $\nabla B$  of 93.8 T/m which is corresponding to magnetophoretic force of 0.203 fN. In comparison, the same particle is experiencing a much weaker magnetophoretic force at 0.038 fN as the separation distance from the magnet pole face increases to 10 mm with magnetic flux density gradient at 17.5 T/m. Therefore, MNPs that experience greater magnetophoretic force will be moving at a higher speed, thus, can be captured and separated from the solution much quickly. Under this scenario, MNPs at the bottom portion of the solution are collected from the aqueous environment much rapidly as the magnetophoresis begins and it is expected to create particle concentration gradient across the suspension from bottom (high  $\nabla B$ ) to top (low  $\nabla B$ ). In fact, this phenomenon will be further amplified by MNPs/MNPs interaction and is well aligned with our previous experimental observation for intensively MNPs/MNPs interacting system.<sup>41</sup> On a side note, this result serves as the best indication in which the continuous homogenization of MNPs suspension is not related to MNPs/MNPs interaction.

However, the non MNPs/Fluid interacting magnetophoresis model simulation result is contradicting with the experimental observation which displays homogeneity throughout the MNPs solution all the time, as described in the previous section. As a consequence, there exists a huge discrepancy between the magnetophoresis separation kinetic profiles obtained from

experiment and predicted by non MNPs/Fluid interacting magnetophoresis model (Fig. 5b). Two major differences between experimental and simulation result are: (1) MNPs were always homogeneously distributed throughout the whole solution in the experiment (Fig. 3b and Fig. 4) while apparent non-uniformity was observed in the model simulation result and is implied by the location dependency of the separation kinetic profile (Fig. 5a and Fig. 5b); (2) MNPs collection time predicted by simulation was much longer compared to the experimental result. This peculiar observation indicates the failure of classical non MNPs/Fluid interacting magnetophoresis model in predicting the separation kinetic profile for our model system.

The homogeneity of MNPs solution demonstrates that there is a driving force which distributes MNPs all over the solution throughout magnetophoresis. This driving force is probably contributed by the fluid convection which usually portrayed as a vital role in agitating or mixing of a solution. Since the surrounding fluid is non-magnetically responsive, it must obtains momentum from the MNPs motion to initiate the convection under magnetophoresis. Hence, there should be some kind of interaction between MNPs and fluid (hydrodynamic interaction) such that momentum from moving MNPs can be transferred to the surrounding fluid and leads to the occurrence of convection. Subsequently, this finding has led us to believe the importance of hydrodynamic effects, originated from MNPs/Fluid interaction might be the predominating factor in homogenizing the MNPs suspension and later accelerate the magnetophoretic capture of MNPs.

### 4.4 Magnetophoresis induced convection

Dye-tracing experiment was performed to trace the fluid motion in the MNPs solution while it is undergoing magnetophoresis. A controlled experiment was also being conducted by using a blank solution (with 0 mg/L of MNPs). It was observed that for the controlled experiment the injected dye at the bottom of the solution

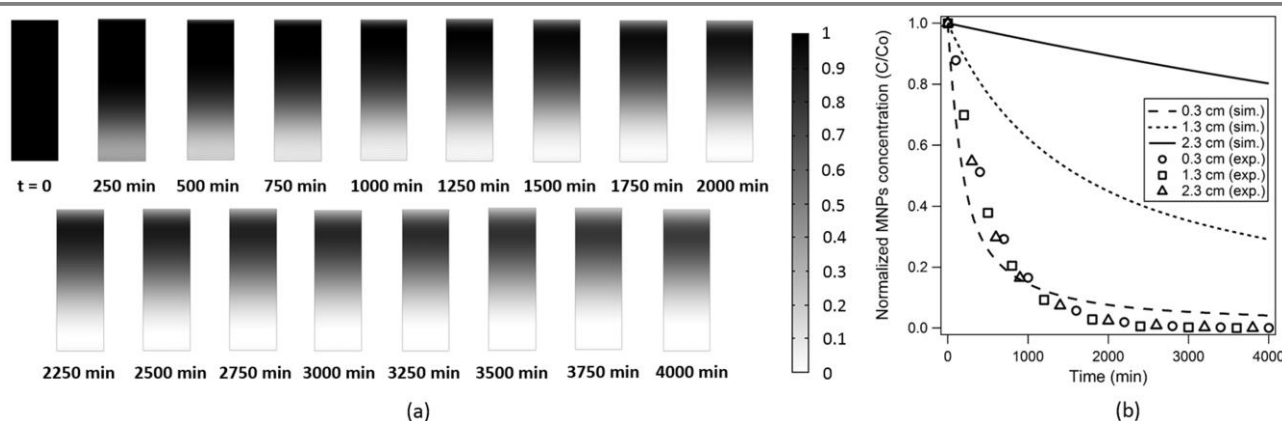


**Fig. 5** (a) Time lapse images of MNPs solution generated by non MNPs/Fluid interacting magnetophoresis model simulation for the first 500 minutes after being subjected to magnetophoresis. The model simulation was carried out by COMSOL Multiphysics. The colorbar indicates the normalized MNPs concentration in the surface plots of MNPs solution, which is ranging from 0 (MNPs concentration is zero) to 1 (initial MNPs concentration before subjecting to magnetophoresis). (b) Comparison between separation kinetic profiles simulated by COMSOL Multiphysics according to non MNPs/Fluid interacting magnetophoresis model (sim.) and obtained from experiment (exp.) at different vertical positions along the cuvette.

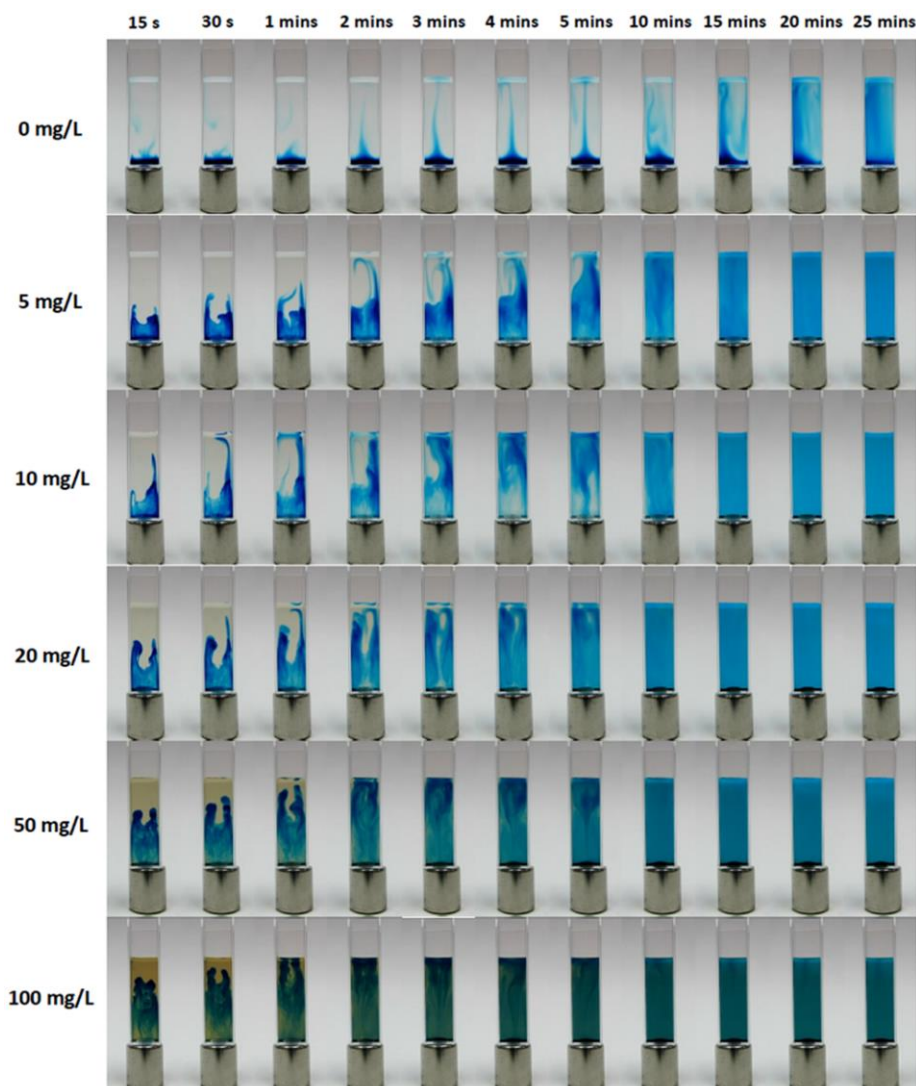


**Fig. 6** Time lapse images for MNPs solution, which has been injected with 3000 mg/L of MB, with different concentration (ranging from 0 to 100 mg/L) for first 25 minutes after being subjected to magnetophoresis. The images in the first row illustrate the dye motion within a blank solution exposed to an external magnetic field, which was used as controlled experiment.

diffused slowly and gradually filled up the whole solution due to the thermal energy without any occurrence of magnetophoresis.<sup>44</sup> For all other MNPs solution, the dye moved upward relatively fast and filled up the solution in a much more rapid pace under magnetophoresis (Fig. 6). The instantaneous migration of the dye in MNPs solution after its exposure to external magnetic field further indicates that convection is generated in MNPs solution during magnetophoresis. This convective flow induces mixing process and has further enhanced the dispersion of MNPs inside the solution and homogenized the suspension, as observed in the experiment described in previous sections (Fig. 3b and Fig. 4). In addition, as depicted in Fig. 6, the dye homogenization is more rapid as the MNPs concentration is higher, as a result of stronger convective flux under magnetophoresis. Moreover, the decline of standard deviation of light intensity throughout the MNPs solution, as shown in Fig. 7, further confirmed the homogenization of the solution as time progresses. Also, it can be observed that dye homogenization rate

(which is equivalent to the rate of decay of light intensity standard deviation) increases with concentration of MNPs solution. Therefore, according to this analysis, convection is more vigorous in more concentrated MNPs solution that is undergoing magnetophoresis, which is consistent with time lapse images displayed in Fig. 6. Based on this observation, it can be deduced that convective motion which occurs during the magnetophoresis of MNPs is also a MNPs concentration dependent phenomenon. The unique feature of magnetophoresis, in which the fluid convection is induced as a consequence of the MNPs/Fluid interaction throughout the process, is not well documented and is the focus of the following discussion.

Macroscopically, the occurrence of fluid convection during magnetophoresis of MNPs solution can be rationalized by using magnetic buoyancy concept. Magnetic buoyancy is defined as force exerted on an object that is immersed in a fluid, in which the surrounding fluid has higher volumetric magnetization compared to

**Table 1** Analogous comparison between natural convection and magnetophoresis.

Process	Illustration	'Substance' to be transferred	Type of field	Driving force	Fluid property which induces convection
Natural convection		Heat energy	Gravitational field	Temperature gradient	Volume per unit mass
Magnetophoresis		MNPs	Magnetic field	Concentration gradient	Magnetization per unit mass

the object itself, under an externally applied magnetic field (Fig. 8a).<sup>45</sup> This magnetic buoyancy concept has been demonstrated by the migration of non-magnetic particles, which are immersed in MNPs solution, in the opposite direction to the magnetic source (magnet) when the MNPs solution is subjected to magnetophoresis.<sup>46, 47</sup> By taking the underlying principle of buoyancy as reference, there is an analogy that can be drawn between natural convection of fluid above a horizontal heating plate and magnetophoresis of MNPs under our experiment condition (Table 1). When a fluid is in thermal contact with a hot horizontal plate, temperature of the fluid layer in the vicinity of the contacted surface increases, the fluid becomes less dense and experiences lower gravitational force per unit volume compared to the surrounding fluid. Thus, the bottom layer of the fluid is driven upwards by gravitational buoyancy force. As the hot

fluid with less density moving upward, the cooler fluid at the top moves down to replace it and complete the flow cycle which causes convectively driven fluid circulation. Likewise, the convective flow in magnetophoresis of MNPs solution can also be explained in a similar manner. Since MNPs tend to be attracted towards region with higher magnetic flux density, MNPs at the bottom of the solution are continuously depleted (captured on the cuvette wall) due to magnetophoretic collection. This condition causes the temporary decline of MNPs concentration and hence reduction of volumetric magnetization of the bottom portion of the solution. Consequently, magnetic force per unit volume experienced by this portion of MNPs solution is relatively lower compared to that of the upper portion of the MNPs solution.<sup>39</sup> Henceforth, the MNPs solution with lower volumetric magnetization is driven upwards by magnetic buoyancy force so that fluid at the upper portion moves down to replace it. By this way the convective current is generated in MNPs solution during magnetophoresis which is consistent with the experimental observation (Fig. 6). This scenario is in fact the driving mechanism for continuous homogenization of the solution which causes the uniform distribution of MNPs as magnetophoresis proceeds (Fig. 4).

In conjunction with the case of natural convection, the significance of magnetophoresis induced convection are dictated by magnetic buoyancy and viscous force. In order to have a better quantitative characterization of these two forces under the context of magnetophoresis induced convection, a new concept known as magnetic Grashof number  $Gr_m$  is introduced. Conventionally Grashof number is a dimensionless number used to represent ratio of buoyancy force to viscous force in a natural convective flow system, which is given by:<sup>48</sup>

$$Gr = \frac{|g| \frac{1}{V} \left( \frac{\partial V}{\partial T} \right)_p (T_s - T_\infty) L_c^3}{\nu^2} \quad (21)$$

where  $V$  is volume per unit mass,  $T_s$  is the temperature of the heating plate,  $T_\infty$  is the bulk temperature of the fluid,  $L_c$  is the characteristic length and  $\nu$  is the kinematic viscosity of fluid. In order to analogously define Grashof number in the magnetophoresis system, the classical Grashof number for natural convection system was

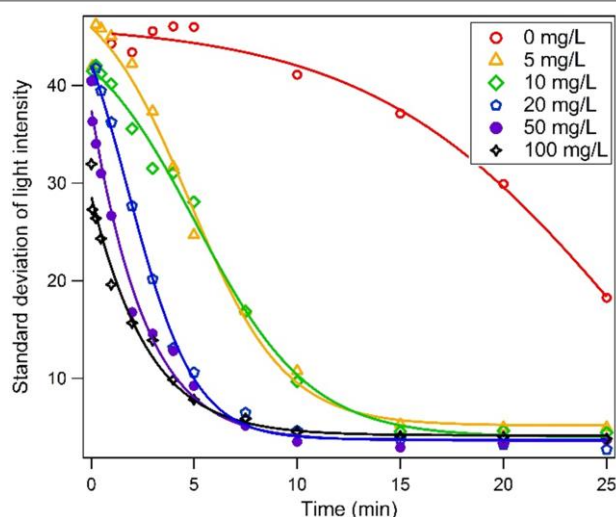


**Fig. 7** Evolution of light intensity standard deviation throughout the MNPs solution (calculated from about 85,000 pixels) with time. The image analysis was performed by Image J. The lower the light intensity standard deviation, the smaller the dispersion of light intensity and hence the more uniform is the dye distribution in MNPs solution. The continuous lines are inserted to guide the eyes.

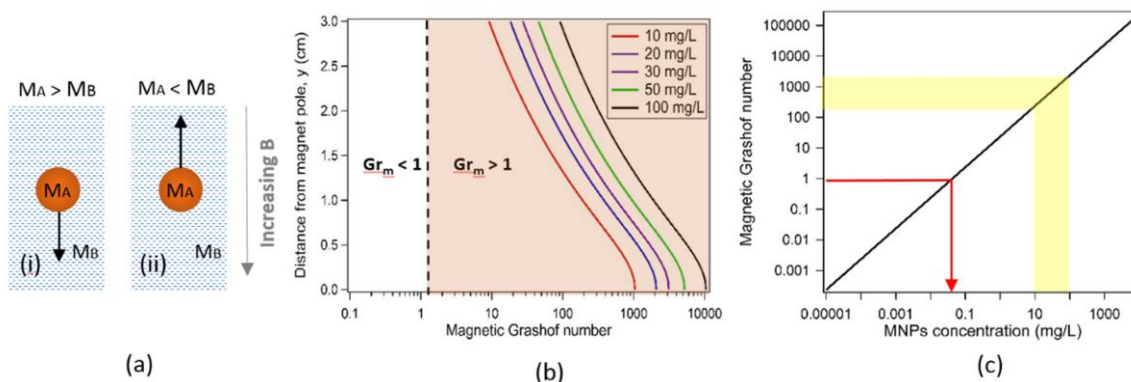


**Fig. 8** (a) (i) When a more magnetically responsive object is immersed in a fluid with lower volumetric magnetization is exposed to an external magnetic field, the object will be driven to the region where magnetic flux density is higher. (ii) In contrast, if the surrounding fluids is more magnetically responsive than the immersed object, the object will experience a negative magnetic force which drives it to region where magnetic flux density is relatively lower. This opposite force is generally known as magnetic buoyancy. (b) The plot of distance from magnet pole against magnetic Grashof number of MNPs solution at different MNPs concentrations. The magnetic Grashof number is calculated according to the experimental configuration in current study. (c) The graph of magnetic Grashof number against MNPs concentration. The calculation was done by adopting the average magnetic flux density gradient in the experimental setup illustrated in Fig. 1. Magnetic Grashof number can only be less than unity provided the concentration of MNPs solution is below 0.05 mg/L (red arrow).

broken down into five parts: (1) force (gravitational force) experienced by a unit mass of fluid under a force field (gravitational field), (2) fractional change of fluid property (volume per unit mass) with respect to another fluid property (temperature) which induces the buoyancy effect to the fluid, (3) driving force for transportation, (4) characteristic length and (5) kinematic viscosity of fluid. Table 2 shows the breakup of the Grashof number as stated above. Likewise, magnetic Grashof number,  $Gr_m$  is analogously defined according to the five parts of Grashof number division as listed in the third column of Table 2. Hence,  $Gr_m$  is given by:

$$Gr_m = \frac{\nabla B \left( \frac{\partial M}{\partial c} \right)_H (c_s - c_\infty) L_c^3}{\rho v^2} \quad (22)$$

Here,  $M$  is magnetization per unit mass of MNPs solution,  $c$  is concentration of MNPs solution,  $c_s$  is MNPs concentration of the surface adjacent to the magnet,  $c_\infty$  is bulk MNPs concentration of the MNPs solution,  $L_c$  is characteristic length,  $\rho$  is density of MNPs solution and  $v$  is kinematic viscosity of the MNPs solution. The magnetophoresis induced convection is noteworthy if  $Gr_m$  is larger than unity.

**Table 2** Breakup of classical Grashof number into five parts in order to facilitate the analogous derivation of magnetic Grashof number

Part	Natural Convection	Magnetophoresis
1	$ g $	$\frac{M \nabla B}{\rho}$
2	$\frac{1}{V} \left( \frac{\partial V}{\partial T} \right)_P$	$\frac{1}{M} \left( \frac{\partial M}{\partial c} \right)_H$
3	$T_s - T_\infty$	$c_s - c_\infty$
4	$L_c$	$L_c$
5	$v$	$v$

Since  $Gr_m$  is the function of  $\nabla B$ , its magnitude decreases with respect to the separation distance from the magnet pole due to the rapid decay of  $\nabla B$  (Fig. 8b). However, even at very low MNPs concentration of 10 mg/L,  $Gr_m$  of the solution is still greater than unity. It follows that magnetophoresis induced convection is inevitable and serves as a critical element which influences the dynamical behavior of the magnetophoresis process in this experiment. According to Equation (17), it is apparent that  $Gr_m$  is also dependent on concentration of MNPs solution subjected to magnetophoresis (Fig. 8c). With higher  $Gr_m$  value, the convective flow becomes more vigorous in concentrated MNPs solution and this analysis is consistent with our experimental observation as indicated in Fig. 6 and Fig. 7. Furthermore, according to our calculation,  $Gr_m$  is less than unity only when the MNPs concentration is smaller than 0.05 mg/L. However, this concentration is too low to be useful for any engineering practical purpose. Therefore, magnetophoresis induced convection always be significant for any kind of engineering application that involves LGMS.

#### 4.5 Hydrodynamically interacting magnetophoresis model

The magnetophoresis induced convection demonstrates the significance of MNPs/Fluid interaction in governing transport behavior of MNPs under a magnetic field. This is the main reason for the failure of non MNPs/Fluid interacting magnetophoresis model to describe the real time magnetophoresis process precisely. Consequently, hydrodynamically interacting magnetophoresis model, which takes MNPs/Fluid interaction into consideration, was developed (Section 3.2) to predict the separation kinetic profile of MNPs solution undergoing low gradient magnetophoresis. Indeed the simulation result from this model shows good agreement with the experimental observation (Fig. 9a), which implies the significance of MNPs/Fluid interaction throughout LGMS. There are two important features which can be noticed from the simulation result by using hydrodynamically interacting magnetophoresis

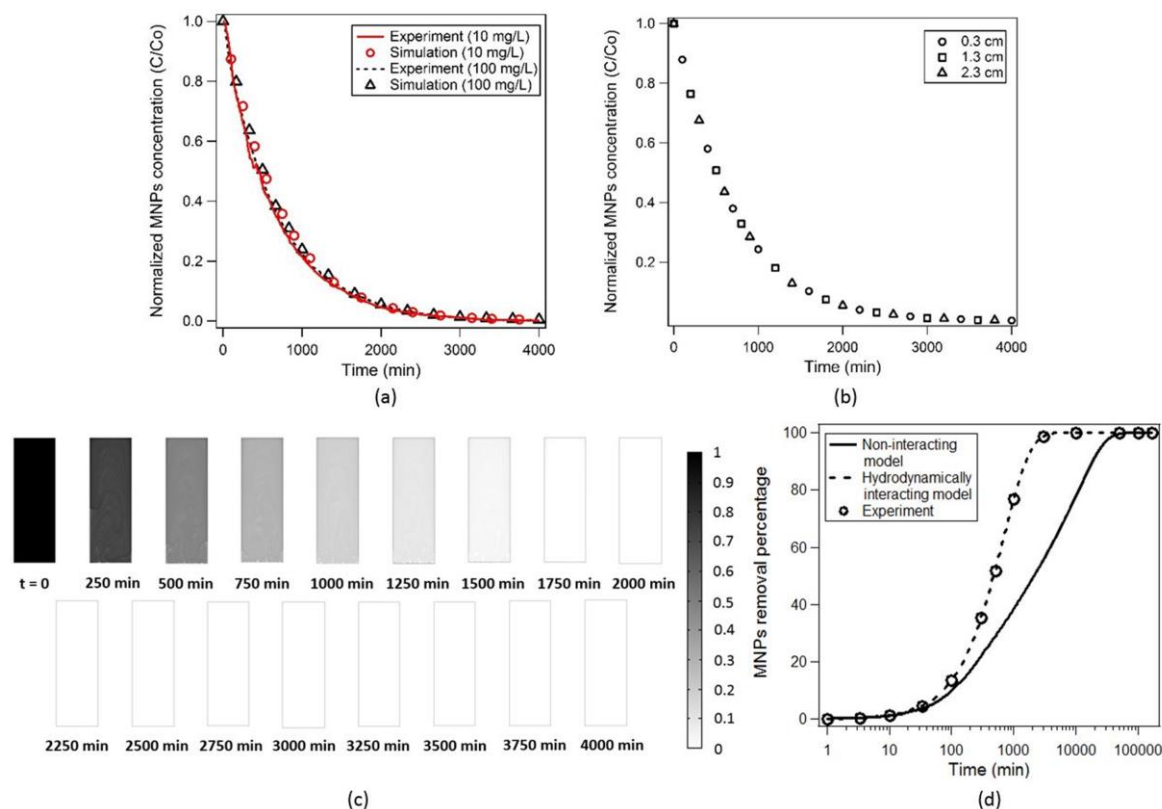


**Fig. 9** (a) Comparison between experimental and simulation result. The simulation result is generated by COMSOL Multiphysics according to hydrodynamically interacting magnetophoresis model. The normalized MNPs concentration is probed at the position which is vertically 2.3 cm away from the magnet pole. (b) Comparison between separation kinetic profiles (predicted from simulation of hydrodynamically interacting magnetophoresis model) at three different locations of MNPs solution where vertical distances from the magnet pole are given by 0.3 cm, 1.3 cm and 2.3 cm respectively. Initial MNPs concentration of 10 mg/L is adopted in this simulation. (c) Time lapse images of MNPs solution generated by COMSOL Multiphysics based on the simulation result from hydrodynamically interacting magnetophoresis model. The colorbar indicates the normalized MNPs concentration in the surface plots of MNPs solution. (d) Comparison between MNPs removal profile predicted by non MNPs/Fluid interacting magnetophoresis model and hydrodynamically interacting magnetophoresis model. The experimental result agrees with the simulation result from hydrodynamically interacting magnetophoresis model.

model. The first feature is the uniform distribution of MNPs throughout the entire solution during magnetophoresis regardless at which position the MNPs concentration is recorded (Fig. 9b). This simulation results is consistent with our previous experiment showing constant separation kinetic profile with respect to spatial distribution in Fig. 3b. For instance, according to the simulation result from non MNPs/Fluid interacting magnetophoresis model, at the moment 500 minutes after the magnetophoresis started, the normalized MNPs concentration is given by 0.2522, 0.7531 and 0.9546 at the positions with vertical distance of 4 mm, 13 mm and 23 mm from the magnet pole respectively. On the contrary, the hydrodynamically interacting magnetophoresis model predicts that the normalized MNPs concentration is given by 0.4748, 0.4643 and 0.4705 at the three given positions in the same moment. These values are close to each other and this indicates that MNPs are almost uniformly distributed throughout the whole solution. The second feature is the occurrence of convective flow in the MNPs solution during magnetophoresis process (Fig. 9c) with its convective rate is dependent upon particle concentration. According to our simulation result, convective flow ranging from  $10^{-5}$  to  $10^{-4}$  m/s is induced in the magnetophoresis of MNPs solution with

concentration of 10 mg/L. The occurrence of induced convective flow indicates that fluid possesses momentum throughout magnetophoresis. For instance, the momentum in this system is originated from the magnetic force that is acting upon MNPs suspended in the solution under an external magnetic field. Due to the viscous property of the surrounding fluid, momentum is transferred into it when velocity gradient presents in the solution and the fluid starts to flow. The two important features mentioned above are observed in our experiment, as described in previous sections. Agreement between our experiment and simulation result is confirmed the importance of MNPs/Fluid interaction in dictating the LGMS performance.

Apart from that, it is desired to study the effect of MNPs/Fluid interaction on the magnetophoretic capture rate of MNPs during low-magnetic field gradient magnetophoresis. As shown in Fig. 9d, it can be observed that the induced convection accelerates the magnetophoretic collection rate of MNPs (hydrodynamically interacting magnetophoresis model) in comparison to the system in which the surrounding fluid remains stagnant (non MNPs/Fluid interacting magnetophoresis model). Based on the simulation result

from non MNPs/Fluid interacting magnetophoresis model, approximately 85,000 minutes is required to achieve 99% of MNPs removal. In contrast, the separation time is greatly reduced to 3,100 minutes according to the simulation result from hydrodynamically interacting magnetophoresis model, which is about 27 times faster compared to the result predicted by non MNPs/Fluid interacting magnetophoresis model. The rapid magnetophoretic capture rate is mainly due to the continuously sweeping of the MNPs that are located far away from the magnet, where  $\nabla B$  is relatively lower, to the region closer to the magnet where it experiences much stronger magnetic force by magnetophoresis induced convection and are separated from the solution within a shorter time scale. By this way, MNPs/Fluid interaction has greatly altered the dynamical behavior of magnetophoresis, accelerates the magnetic separation process and improves the practicability of LGMS in engineering application.

## 5 Conclusion

We have revealed the pivotal role of sweeping flow created from MNPs convection in self-dispersing the MNPs during the magnetophoresis process. Even at an extremely diluted MNPs solution with concentration of 10 mg/L, in which MNPs/MNPs interaction is negligible, this hydrodynamic driven phenomenon is still nontrivial. The continuous dispersion of MNPs into the suspension is leading to the homogenous distribution of MNPs across the entire solution and greatly influences dynamical behavior of LGMS. One of the most significant advantages contributed by MNPs/Fluid interaction to LGMS is the more rapid magnetophoretic capture of MNPs during magnetophoresis. We believe by taking advantage of this scenario, it is possible to overcome one of the most significant problems in implementing LGMS for large scale engineering application, which is the extremely rapid decay of  $\nabla B$  with the distance from the magnet leading to poor separation performances of LGMS.<sup>43</sup> In the case of cooperative magnetophoresis (under MNPs/MNPs interacting mode),<sup>22</sup> we anticipated that the influence of hydrodynamic effect is dependent on MNPs concentration. At moderate to high MNPs concentration, magnetophoresis induced convection creates agitation within MNPs solution and enhances the mixing of MNPs, which in turn promotes the acceleration of MNPs aggregation and magnetophoretic separation. For extreme cases with extremely high MNPs concentration, we anticipated that 'cooperative factors' would overwhelm the hydrodynamic effects mainly due to the (1) high aggregation kinetic of MNPs, and, (2) larger MNPs cluster size formed, which leads to speedy motion of cluster under magnetophoresis. In conclusion, MNPs/Fluid interaction (which is generally known as hydrodynamic interaction) is the influential fundamental interaction that controls the magnetophoretic behavior of MNPs solution that is undergoing magnetophoresis and it should be taken into consideration in the modeling of magnetophoresis process and design of magnetic separator.

## Acknowledgements

Sim Siong Leong acknowledges the support from the Ministry of Higher Education of Malaysia through the MyPhD Scholarship. This project was also financially supported by

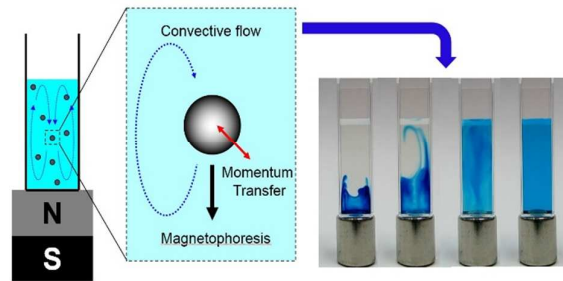
Research University grant from USM (Grant no. 1001/PJKIMIA/811219) and FRGS grant from MOHE (Grant no. 203/PJKIMIA/6071269). We gratefully acknowledge Prof. Tim St Pierre from University of Western Australia for the discussion on magnetic buoyancy force.

## References

1. Q. A. Pankhurst, J. Connolly, S. K. Jones and J. Dobson, *J. Phys. D: Appl. Phys.*, 2003, **36**, R167.
2. A. K. Gupta and M. Gupta, *Biomaterials*, 2005, **26**, 3995-4021.
3. J. Dobson, *Gene Ther.*, 0000, **13**, 283-287.
4. W. H. De Jong and P. J. A. Borm, *Int. J. Nanomedicine*, 2008, **3**, 133-149.
5. K. E. McCloskey, J. J. Chalmers and M. Zborowski, *Anal. Chem.*, 2003, **75**, 6868-6874.
6. M. Zborowski and J. J. Chalmers, *Anal. Chem.*, 2011, **83**, 8050-8056.
7. C. T. Yavuz, A. Prakash, J. T. Mayo and V. L. Colvin, *Chem. Eng. Sci.*, 2009, **64**, 2510-2521.
8. Y. F. Shen, J. Tang, Z. H. Nie, Y. D. Wang, Y. Ren and L. Zuo, *Sep. Purif. Technol.*, 2009, **68**, 312-319.
9. I. Akin, G. Arslan, A. Tor, M. Ersoz and Y. Cengeloglu, *J. Hazard. Mater.*, 2012, **235-236**, 62-68.
10. P. Xu, G. M. Zeng, D. L. Huang, C. L. Feng, S. Hu, M. H. Zhao, C. Lai, Z. Wei, C. Huang, G. X. Xie and Z. F. Liu, *Sci. Total Environ.*, 2012, **424**, 1-10.
11. S. C. N. Tang and I. M. C. Lo, *Water Res.*, 2013, **47**, 2613-2632.
12. V. Schaller, U. Kräling, C. Rusu, K. Petersson, J. Wipenmyr, A. Krozer, G. Wahnström, A. Sanz-Velasco, P. Enoksson and C. Johansson, *J. Appl. Phys.*, 2008, **104**, 093918.
13. A. F. Pshenichnikov and A. S. Ivanov, *Phys. Rev. E*, 2012, **86**, 051401.
14. J. Gómez-Pastora, E. Bringas and I. Ortiz, *Chem. Eng. J.*, 2014, **256**, 187-204.
15. J. Lim, C. Lanni, E. R. Evarts, F. Lanni, R. D. Tilton and S. A. Majetich, *ACS Nano*, 2010, **5**, 217-226.
16. G. D. Moeser, K. A. Roach, W. H. Green, T. Alan Hatton and P. E. Laibinis, *AIChE J.*, 2004, **50**, 2835-2848.
17. P. Y. Toh, S. P. Yeap, L. P. Kong, B. W. Ng, D. J. C. Chan, A. L. Ahmad and J. K. Lim, *Chem. Eng. J.*, 2012, **211-212**, 22-30.
18. G. Mariani, M. Fabbri, F. Negrini and P. L. Ribani, *Sep. Purif. Technol.*, 2010, **72**, 147-155.
19. C. T. Yavuz, J. T. Mayo, W. W. Yu, A. Prakash, J. C. Falkner, S. Yean, L. Cong, H. J. Shipley, A. Kan, M. Tomson, T. Natelson and V. L. Colvin, *Science*, 2006, **314**, 964-967.
20. G. De Las Cuevas, J. Faraudo and J. Camacho, *J. Phys. Chem. C*, 2008, **112**, 945-950.
21. L. E. Helseth and T. Skodvin, *Meas. Sci. Technol.*, 2009, **20**, 095202.
22. J. Faraudo and J. Camacho, *Colloid Polym. Sci.*, 2010, **288**, 207-215.
23. J. S. Andreu, J. Camacho, J. Faraudo, M. Benelmekki, C. Rebollo and L. M. Martínez, *Phys. Rev. E*, 2011, **84**, 021402.

24. J. S. Andreu, J. Camacho and J. Faraudo, *Soft Matter*, 2011, **7**, 2336-2339.
25. J. S. Andreu, P. Barbero, J. Camacho and J. Faraudo, *J. Nanomat.*, 2012, **2012**, 5-5.
26. J. Faraudo, J. S. Andreu and J. Camacho, *Soft Matter*, 2013, **9**, 6654-6664.
27. Y. Xu, Y. Qin, S. Palchoudhury and Y. Bao, *Langmuir*, 2011, **27**, 8990-8997.
28. R. Lakshmanan, C. Okoli, M. Boutonnet, S. Järås and G. K. Rajarao, *Bioresource Technol.*, 2013, **129**, 612-615.
29. R. Lakshmanan, M. Sanchez-Dominguez, J. A. Matutes-Aquino, S. Wennmalm and G. Kuttuva Rajarao, *Langmuir*, 2014, **30**, 1036-1044.
30. S. A. Khashan, E. Elnajjar and Y. Haik, *J. Magn. Magn. Mater.*, 2011, **323**, 2960-2967.
31. S. A. Khashan and E. P. Furlani, *Microfluid. Nanofluid.*, 2012, **12**, 565-580.
32. S. A. Khashan and E. P. Furlani, *J. Phys. D: Appl. Phys.*, 2013, **46**, 125002.
33. S. A. Khashan and E. P. Furlani, *Sep. Purif. Technol.*, 2014, **125**, 311-318.
34. S. A. Khashan, A. Alazzam and E. P. Furlani, *Sci. Rep.*, 2014, **4**, 5299.
35. J. Lim, S. Yeap, H. Che and S. Low, *Nanoscale Res. Lett.*, 2013, **8**, 381.
36. Z. Zhang and J. Kong, *J. Hazard. Mater.*, 2011, **193**, 325-329.
37. E. P. Furlani and K. C. Ng, *Phys. Rev. E*, 2008, **77**, 061914.
38. G. P. Hatch and R. E. Stelter, *J. Magn. Magn. Mater.*, 2001, **225**, 262-276.
39. R. E. Rosensweig, *Ferrohydrodynamics*, Dover Publications, New York, 2014.
40. R. B. Bird, W. E. Stewart and E. N. Lightfoot, *Transport Phenomena*, Wiley, New York, 2006.
41. J. Lim, S. P. Yeap and S. C. Low, *Sep. Purif. Technol.*, 2014, **123**, 171-174.
42. S. P. Yeap, S. S. Leong, A. L. Ahmad, B. S. Ooi and J. Lim, *J. Phys. Chem. C*, 2014, **118**, 24042-24054.
43. J. Lim, S. P. Yeap and S. C. Low, *Sep. Purif. Technol.*, 2014, **123**, 171-174.
44. H. C. Berg, *Random Walks in Biology*, Princeton University Press, Chichester, 1993.
45. K. Henjes, *Z. Physik B - Condensed Matter*, 1993, **92**, 113-127.
46. R. M. Erb, H. S. Son, B. Samanta, V. M. Rotello and B. B. Yellen, *Nature*, 2009, **457**, 999-1002.
47. M. Benelmekki, L. M. Martinez, J. S. Andreu, J. Camacho and J. Faraudo, *Soft Matter*, 2012, **8**, 6039-6047.
48. J. P. Holman, *Heat Transfer*, McGraw-Hill, New York, 2008.

## Table of content



Experimental and theoretical studies on nanoparticle-fluid interaction in dictating low gradient magnetophoresis of magnetic nanoparticles